OPEN

ASAIO Journal 2022

Multilayer Scaling of a Biomimetic Microfluidic Oxygenator

Else M. Vedula,* Brett C. Isenberg,* Jose Santos,* WeiXuan Lai,* Diana J. Lewis,* David Sutherland,* Teryn R. Roberts,† George T. Harea,† Christian Wells,* Bryan Teece,* Joseph Urban,* Thomas Risoleo,* Derek Solt,‡ Sahar Leazer,§ Kevin Chung,§ Sivaprasad Sukavaneshvar,‡ Andriy I. Batchinsky,† and Jeffrey T. Borenstein*

Abstract Extracorporeal membrane oxygenation (ECMO) has been advancing rapidly due to a combination of rising rates of acute and chronic lung diseases as well as significant improvements in the safety and efficacy of this therapeutic modality. However, the complexity of the ECMO blood circuit, and challenges with regard to clotting and bleeding, remain as barriers to further expansion of the technology. Recent advances in microfluidic fabrication techniques, devices, and systems present an opportunity to develop new solutions stemming from the ability to precisely maintain critical dimensions such as gas transfer membrane thickness and blood channel geometries, and to control levels of fluid shear within narrow ranges throughout the cartridge. Here, we present a physiologically inspired multilayer microfluidic oxygenator device that mimics physiologic blood flow patterns not only within individual layers but throughout a stacked device. Multiple layers of this microchannel device are integrated with a three-dimensional physiologically inspired distribution manifold that ensures smooth flow throughout the entire stacked device, including the critical entry and exit regions. We then demonstrate blood flows up to 200 ml/min in a multilayer device, with oxygen transfer rates capable of saturating venous blood, the highest of any microfluidic oxygenator, and a maximum blood flow rate of 480 ml/min in an eight-layer device, higher than any yet reported in a microfluidic device. Hemocompatibility and large animal studies utilizing these prototype devices are planned.

Supplemental Visual Abstract, http://links.lww.com/ASAIO/A769. *ASAIO Journal* 2022; 68;1312–1319

Key Words: microfluidics, oxygenator, transfer, scaling, multilayer

From the *Draper, Cambridge, Massachusetts; †Autonomous Reanimation and Evacuation (AREVA) Research Program, The Geneva Foundation, San Antonio, Texas; ‡Thrombodyne, Inc., Salt Lake City, Utah; and §Uniformed Services University of the Health Sciences, Bethesda, Maryland.

Submitted for consideration June 2021; accepted for publication in revised form November 2021.

Disclosure: The authors have no conflicts of interest to report.

Supplemental digital content is available for this article. Direct URL citations appear in the printed text, and links to the digital files are provided in the HTML and PDF versions of this article on the journal's Web site (www.asaiojournal.com).

Correspondence: Jeffrey T. Borenstein, PhD, Bioengineering Division, Draper, 555 Technology Square, MS 32, Cambridge MA 02139. Email: jborenstein@draper.com.

DOI: 10.1097/MAT.0000000000001647

Increasing prevalence of acute and chronic lung diseases, combined with limitations and complications associated with mechanical ventilation,[1,2] have spurred intense interest in extracorporeal membrane oxygenation[3–6] (ECMO). A critical need remains for low prime volume, lower flow respiratory support devices with reduced reliance on anticoagulants for neonates.[7–9] There is also an urgent requirement for simpler, safer, and more portable ECMO technologies for the treatment of battlefield injuries in the early post-injury phase before patient transport to definitive care facilities.[10,11] Recent experiences with the 2009 H1N1 pandemic[12] and COVID-19[13,14] have highlighted concerns with mechanical ventilation and are spurring further impetus toward advancements in ECMO technology.

Microfluidic oxygenators have emerged as a potential avenue for improving the efficiency and safety of ECMO, by virtue of the precisely controlled blood path and physiologically relevant dimensions of microchannels and gas transfer membranes in ways that are not achievable by current hollow fiber membrane (HFM) oxygenators.[15–17] These advantages may translate into shorter gas diffusion distances and tighter control over blood flow patterns in microfluidic devices relative to their hollow fiber-based counterparts.[18] However, a remaining challenge for microfluidics-based technologies in medicine is the difficulty encountered when attempting to scale these devices toward blood flow rates required for clinical applications.[19,20]

Microfluidic devices emerged as a platform for lab-on-a-chip devices for applications in clinical diagnostics and bioanalysis, where small fluid volumes and low flow rates are actually a technological advantage,[21] and efforts to apply microfluidic platforms toward therapeutic applications, such as kidney dialysis and respiratory assist, have appeared only recently.[16,17,22–27] Conventional microfluidic fabrication techniques are based upon photolithographic processes that are best suited for small features and rectangular geometries, and are generally limited to a single feature depth in the vertical dimension unless strenuous efforts are made to patch together multiple photomasking, lithographic, and/or etching steps.[28] These considerations have heretofore limited most oxygenator designs to relatively low flow rate prototypes, and larger structures have required stacking of numerous low flow layers together using techniques that are labor-intensive and introduce undesirable flow patterns into the distribution and manifolding regions.

Precision machining technologies capable of generating three-dimensional branching microchannels of varying depths across the network, mimicking the architecture of the *in vivo* microcirculation, represent a promising approach toward scaling microfluidic oxygenators. As reported by Hoganson and Vacanti[26] and our group,[29] these micromachining approaches are capable of generating branching networks in a manner not possible through conventional lithographically based microfluidics. These reports described single-layer oxygenator devices

limited to maximum blood flow rates well under 100 ml/min, spurring interest in scaling the technology in the vertical dimension. A previous report of vertical scaling[30] successfully demonstrated the integration of 32 single oxygenator layers, but utilized square cross-section constant dimension manifold channels and was only able to reach blood flow rates of 48 ml/min in a multilayer configuration.

Here we present a novel approach toward scaling microfluidic oxygenator devices using three-dimensional branching manifolds that integrate multiple stacked layers of oxygen transfer units. Multiple gas transfer units are stacked into a three-dimensional network joined by fully three-dimensional precision-machined blood distribution manifolds, designed to distribute blood uniformly and to control shear within a desired physiologic range across the entire stacked device.

The use of precision machining of the blood distribution manifold enables stacks to be joined while avoiding sharp corners and sudden transition regions that are known to disturb blood flow streamlines. These vertical blood distribution manifolds that join layers are fabricated from directly machined transparent hard plastics, with rounded channel cross-sections and smoothly varying dimensions that carry blood to and from the extracorporeal circuit. At blood flow rates of 200 ml/min in an eight-layer device, gas transfer capable of raising venous blood to 95% oxygen saturation, corresponding to a volume percent transfer of 5 vol%, is demonstrated. This flow rate also corresponds to a shear rate in the gas transfer channels of approximately 250/s, consistent with favorable conditions for blood health in extracorporeal circulation systems. Maximum blood flow rates up to 480 ml/min in an eight-layer device, the highest yet reported for a microfluidic device, are demonstrated, with blood gas transfer measured under multiple blood flow and gas flow conditions. Initial evaluation of the hemocompatibility of this stacked structure microfluidic oxygenator is underway, to evaluate this approach as a step toward safer and more efficacious respiratory assist technology.

Materials and Methods

Computationally Based Device Design

A computational finite element analysis tool (COMSOL, Burlington, MA) was utilized to help drive the design of the device from two aspects, first to optimize the blood flow patterns and second to optimize the gas transfer efficiency. In each case, governing principles included the requirement for carefully controlled fluid shear and pressure drops and the aim to achieve a highly efficient transfer of oxygen while maintaining channel dimensions that could be fabricated using currently available techniques. As described elsewhere, a single gas transfer unit of the microfluidic oxygenator device comprises a network of gas channels, positioned opposite a layer with a network of branching blood channels, and a nonporous gas-permeable layer in between. Each of these three layers is comprised of the highly gas-permeable silicone poly(dimethylsiloxane) (PDMS).

The design of the vascular network layer is aimed at controlling the shear stress on the blood within a narrow window by maintaining smooth, laminar flow while minimizing disruptions to the blood streamlines throughout its entire journey from the inlet distribution manifold, into the large parallel array of gas transfer channels, and exiting at the outlet distribution manifold. This design paradigm has been applied to the vertical manifold that joins multiple channels in a three-dimensional stack arrangement.

The device design invoked here is described elsewhere[29]; briefly, it comprises a layer roughly 20 × 25 cm in the horizontal dimension, encompassing 176 parallel blood channels, each with a width of 500 microns and intervening 500-micron walls, and the length of the channels in the parallel array is 15.1 cm, with transition regions designed to accommodate lengths sufficient to achieve fully developed flow. The blood layer design is shown in **Figure 1**; a similar approach is invoked for the oxygen network design.

Shear rate and blood flow distributions were modeled as described in the Methods, using COMSOL, generating predicted values throughout the microchannel network and the blood distribution manifolds. Modeled shear rates at 200 ml/min blood flow in an eight-layer device, for sections comprising the gas transfer microchannels, are shown in **Figure 2A**, and for the in-layer blood distribution manifold in **Figure 2B**. Shear data obtained from the COMSOL model for the channel regions, bifurcations, and manifold trunk line is provided in Table S1, Supplemental Digital Content 1, http://links.lww.com/ASAIO/A768, along with supplemental details on the fluid dynamic simulations.

A second evaluation of the fluid dynamics of the system was conducted using COMSOL to predict flow streamlines in the system. In **Figure 3A**, flow streamlines through branches of the in-layer blood distribution manifold are shown at low magnification, illustrating the gently curved paths the blood follows along the excursion from the trunk line into the gas transfer channels. **Figure 3B** shows the streamlines at higher magnification, providing further insight into the physiologically inspired flow patterns at branch points.

Device Fabrication

Master molds in aluminum were fabricated with a computer numerical control (CNC) milling machine (Mitsui

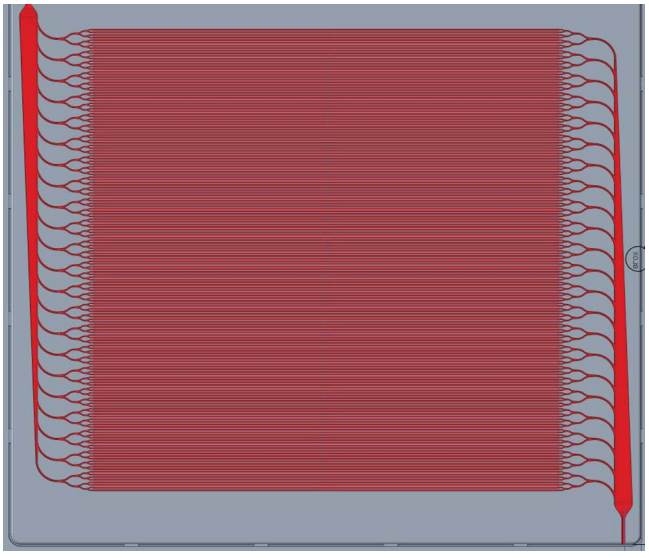

Figure 1. Drawing of single-layer microfluidic oxygenator blood layer, showing in-layer manifolds and 176 parallel blood channels.

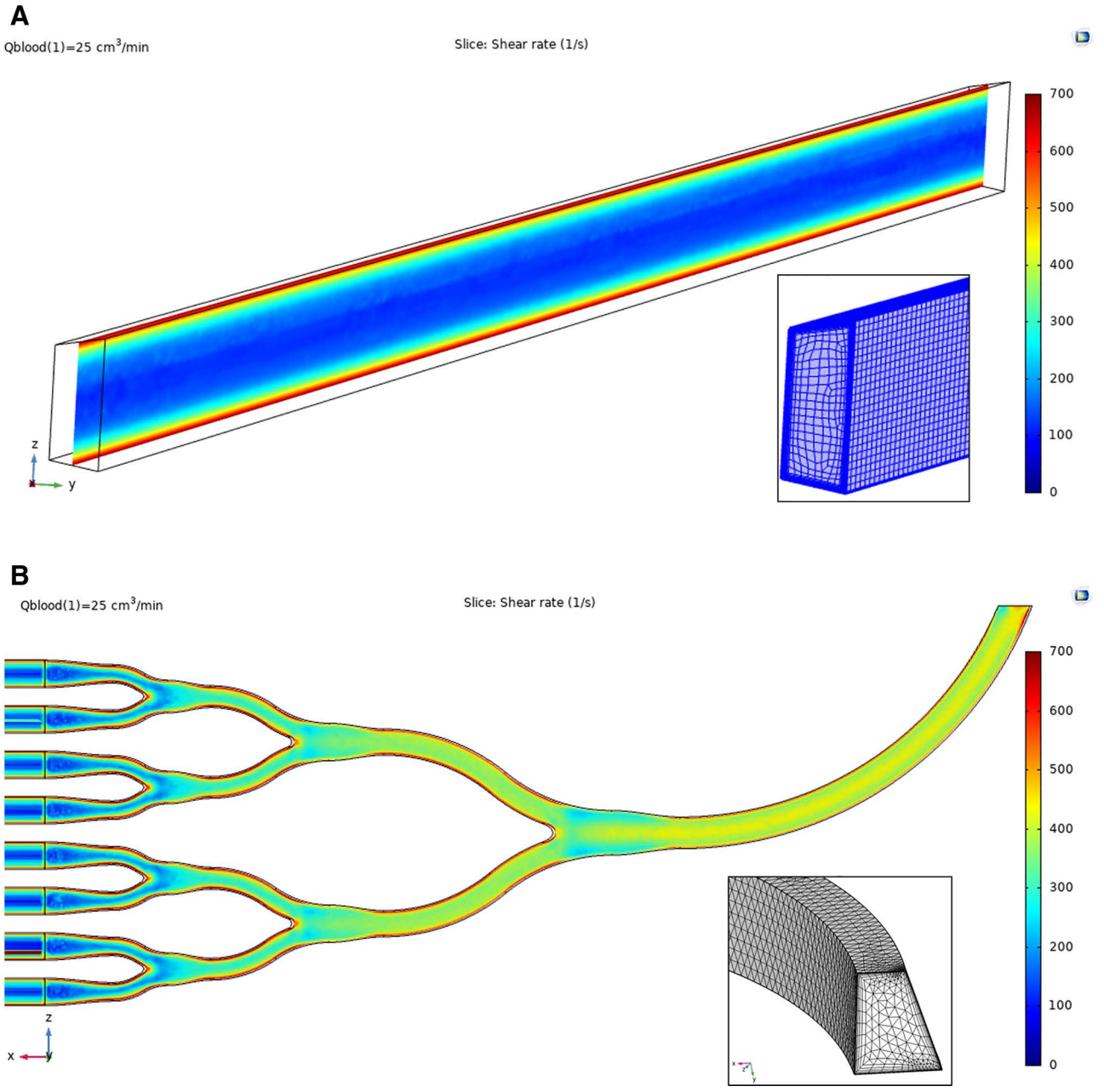

Figure 2. A: False color map of wall shear rate predicted by the COMSOL model across several parallel gas transfer microchannels in the single-layer oxygenator. **B**: Similar COMSOL model predicting wall shear rate across the trunk line and multiple branches of the blood distribution manifold.

Seiki VU50A Machining Center, with positional accuracy of ±0.00004″ at full stroke) to produce an inverse replica of the layer design described above. Blood layer and oxygen layer designs were reverse-machined into aluminum molds for microreplication into the respective microchannel networks. Surface roughness on the CNC-machined Al molds was measured to be less than 0.2 microns on average. The fabrication process for the single-layer device layers is described and illustrated elsewhere.[29]

For these devices, the channel depth was 200 microns and the target gas transfer membrane thickness was 50 microns. We have estimated the thickness of the adhesive layer for membrane attachment, determined by comparing mold dimensions in several locations to the overall channel depth after membrane bonding, at a value of 13 microns on average.

Blood and oxygen layers were bonded using a thin layer of adhesive as described elsewhere.[29] A thin layer of adhesive (DOWSIL 3140 RTV, Dow Silicone Corporation, Midland, MI) was deposited onto a flat surface, followed by transfer to the oxygen layer using an ink roller. This layer was then placed in contact with the open surface of the thin gas transfer membrane while it was still held by the Si wafer, and the layer-membrane bond was cured overnight at 65°C. The same procedure was used to attach the blood layer to the other side of the membrane after the oxygen layer/membrane assembly was fully removed from the Si wafer. Care is taken to avoid any buildup of adhesive

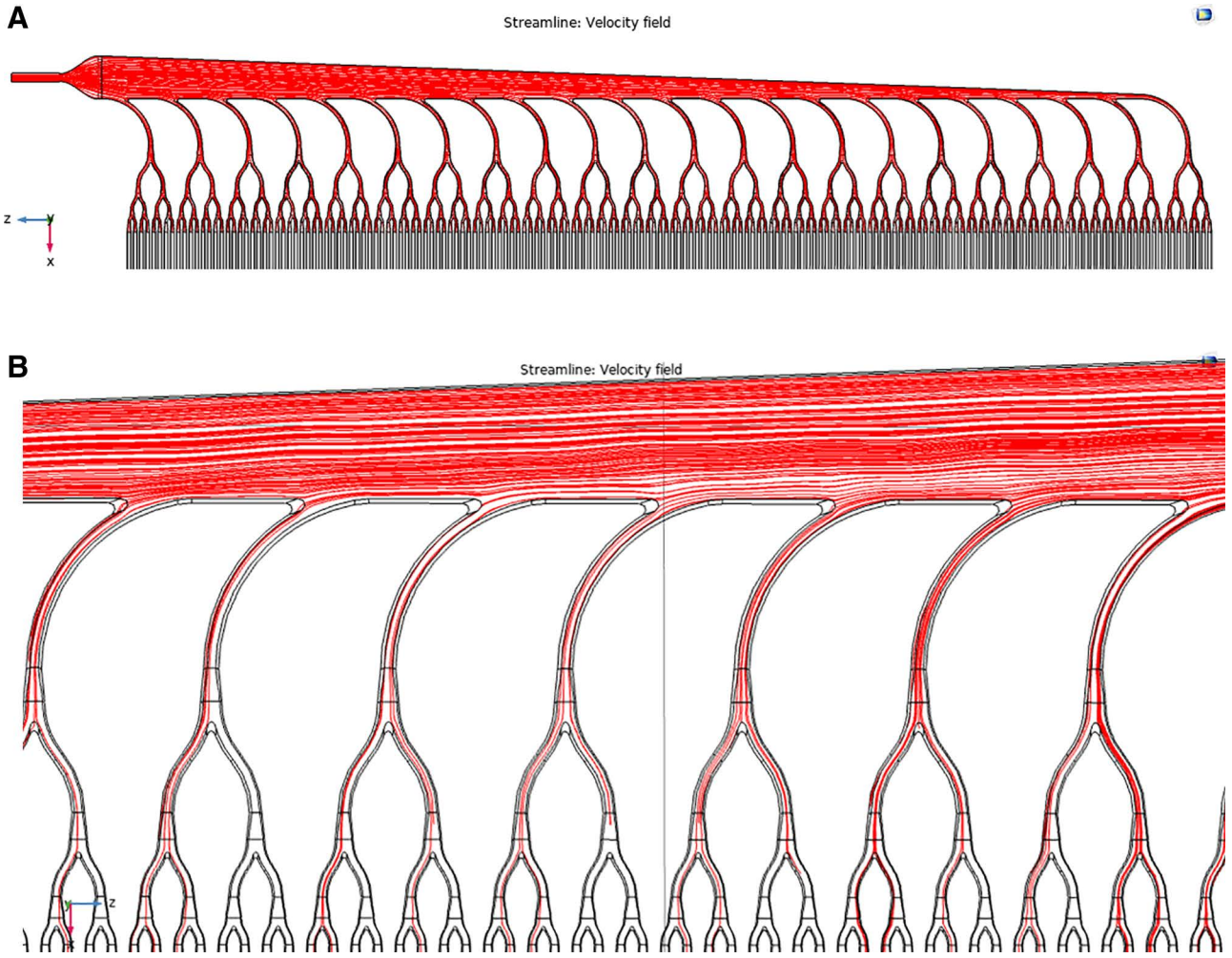

Figure 3. Fabrication process diagram showing the steps involved in constructing and assembling a single layer oxygen layer–membrane–blood layer sandwich structure with tubing connections. **A**: Low magnification map of flow streamlines modeled using COMSOL, showing the patterns of flow in the in-layer distribution manifold. **B**: Higher magnification view of flow streamlines, illustrating patterns of flow exiting the in-layer distribution manifold and entering the arrays of parallel transfer channels.

that might lead to wrinkling of the membrane, and each sandwich structure is carefully inspected to ensure that no wrinkles are present. A perpendicular alignment of the blood and oxygen channels in their respective layers was maintained during the bonding process, so that the oxygen channels effectively crossed each of the blood channels in the design. The assembled stacked structure of the blood layer–membrane–oxygen layer was placed in an oven set to 65°C for at least 1.5 hours.

Individual blood–membrane–oxygen connections were made with 1/32″ ID Tygon tubing (Cole Palmer, Vernon Hills, IL) attached to 1/32″ ID stainless steel tubing (New England Small Tube). A thin layer of uncured PDMS was applied to tubing interfaces followed by curing at 65°C for at least 3 hours, followed by leak and pressure testing.[17]

Fabrication of Eight-layer Stack

After leak and pressure testing, eight fully functional device layers were stacked and aligned so that the blood inlet and outlet ports were in vertical alignment. The inlet and outlet blood manifolds were attached to the individual device layers by connecting the previously attached Tygon tubing to the stainless steel tubes on the manifolds. The manifolds were connected to the testing system *via* Luer lock connectors on the manifolds. The oxygen layers of the eight individual devices were connected in series such that the outlet from layer 1 was connected to the inlet of layer 2. All connections of the oxygen layers were completed using Luer lock connectors.[29]

Manifold Fabrication

Uniform fluid distribution to and from each of the layers of the eight-layer stack was accomplished using a custom 1-to-8 bifurcating vertical manifold. The branching channels were designed to smoothly split or recombine the flow such that the fluid in every branch experiences the same level of shear stress. The manifolds were fabricated by Edge Embossing Inc. (Charlestown, MA) by precision machining the half-channel geometry into two identical pieces of polycarbonate, which were subsequently thermally bonded to each other in a heated press to create the full lumen geometry. To provide connection points to the manifold, a polycarbonate male Luer fitting was glued into the one-port side of the manifold, while 19 XTW gauge 304 stainless steel tubing (New England

Small Tube) was glued into each of the channels on the eight-port side.

Gas Transfer Testing

Blood oxygen transfer testing was conducted as shown in the photograph in **Figure 4**. This testing system for the eight-layer device differed from prior single-layer device testing that utilized a syringe pump, comprising a peristaltic pump (Watson Marlow, Wilmington, MA), a pressure sensor (Pendotech, Princeton, NJ), two pressure controllers (Alicat, Tucson, AZ), heated blood rocker (ThermoScientific, Waltham, MA), and the assembled eight-layer device. The peristaltic pump controlled the blood flow into the device. The pressure sensor monitored the inlet pressure in the vascular channel and was used to measure the pressure drop in mmHg across the device and the tubing connections. The two pressure controllers controlled the inlet and outlet pressure of the oxygen channel. The vascular channel layer of the assembled device was purged and primed with ethanol (EtOH) to remove air bubbles in the device. Connections between the syringe, the device, pressure sensors, and pressure controllers were all Luer lock connections. Connections to the vascular layer were made using the wet-to-wet connection technique with an EtOH prime followed by a saline prime to ensure no air bubbles were introduced in the line.

A pressure controller was connected in line between the oxygen tank and the oxygen inlet of the device. This controller controlled the inlet oxygen flow out of the tank into the device. The blood was tested after it had been passed through the device using a Blood Gas Analyzer (BGA; Instrumentation Laboratory, Bedford, MA), and the Avoximeter (ITC, Edison, NJ). The BGA was used to measure the partial pressure of O_2 in the blood before and during the experiment. The Avoximeter measures the oxyhemoglobin content (percent of hemoglobin saturated by O_2) before and during the experiment. Experiments were performed using porcine blood treated with anticoagulant citrate-phosphate-dextrose (Lampire Biologic Laboratories, Pipersville, PA) and shipped overnight under refrigeration. The blood was heated up to 37°C and conditioned to venous conditions for pH, O_2, and CO_2 concentrations. This conditioning process was accomplished by passing the blood through a loop circuit with a commercial hollow fiber oxygenator until the blood measured 65 ± 5% oxygen saturation, a target value that typically brings the pH and CO_2 concentrations into fairly well-controlled ranges as well. The blood was placed in a heated rocker to prevent clotting and hold the temperature.

Blood was drawn from a transfer bag (Terumo, Tokyo, Japan) into the pump. The blood in the transfer bag was tested with one blood gas reading and three Avoximeter readings before flowing through the device. This established a baseline for the blood going into the device. The oxygen pressure controller was tuned for a 100 ml/min oxygen flow rate. Blood flow rates included 10, 20, and 30 ml/min through a single layer of the microfluidic oxygenators. The flow rates were held for a duration ranging from 2 to 4 minutes. Flow rates were not randomized, but fresh venous blood was introduced before each measurement. Samples of the blood outlet were taken for measurements using the BGA and Avoximeter. One BGA reading and three Avoximeter readings were taken. These measurements were used to calculate the transfer of oxygen from the oxygen layer into the blood layer.

Results

Assembled Device Construction

The eight-layer assembled device structure is shown in **Figure 5** before filling with blood; note the vertical distribution manifold in the foreground. The device was observed to fill smoothly with blood, with the manifold effectively distributing blood through each of the eight horizontal layers simultaneously, by virtue of the manifold design and the resistive network that provided even flow distribution to each layer in rapid sequence. Small bubbles were visible during the initial filling process and were manually tapped out from the layers to eliminate any visible bubbles that might disturb or occlude flow within the network.

Blood Pressure Testing: Experimental and Computational Results

Blood pressure was measured as a function of flow rate in the eight-layer device assembly as described in the Methods section. Results are provided in **Figure 6**, where the markers indicate the experimental data and the solid line shows the predictions of the computational model. Here, we have included the resistance and associated contribution to the pressure drop

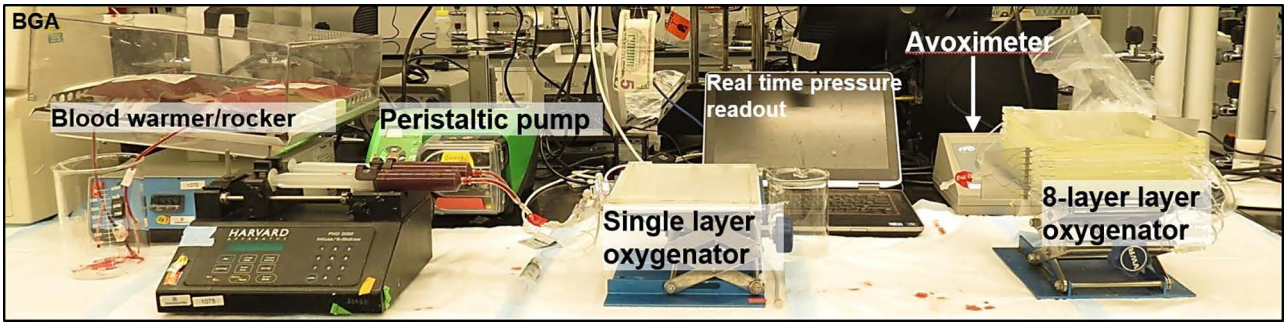

Figure 4. Photograph of test apparatus used to evaluate oxygen transfer in the multilayer microfluidic oxygenator described in the text. Blood gases are measured using a blood gas analyzer (BGA, not shown on the left), and hemoglobin-bound oxygen is measured by a hemoximeter. Blood is pumped with a peristaltic pump (syringe pump also shown as it is used to test single-layer devices) through the device, and pressure drop and blood flow rate are monitored as shown. High purity oxygen is introduced through the gas channel network and the flow rate is measured as shown.

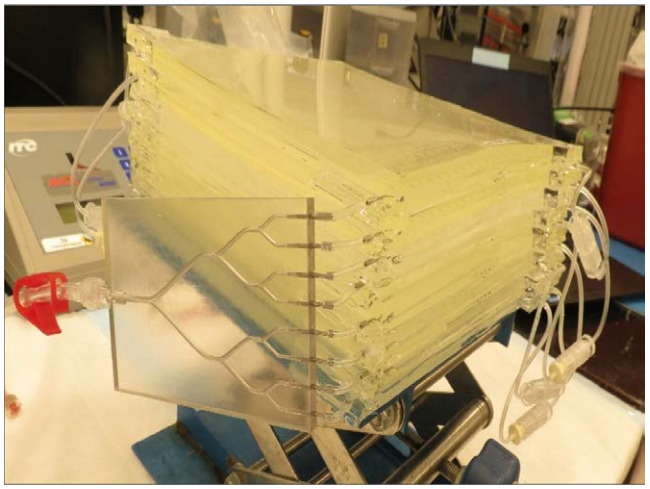

Figure 5. Photograph of the eight-layer microfluidic oxygenator before blood filling featuring inlet blood manifold at front left.

of the vertical manifold and tubing in addition to the layer drop. Note that the resistive losses in the manifold and tubing connections are roughly equivalent to those observed in the layers.

Oxygen Transfer Testing: Experimental and Computational Results

Blood gas oxygen transfer testing was conducted on a single eight-layer stack device, using methods as described in the Methods section. Given the very high volumes of blood required, testing needed to be carried out very efficiently to capture multiple oxygen transfer data points across a range of blood flow rates in this device. The oxygen transfer data is shown in **Figure 7**, where the oxygen transfer is plotted in volume percent transfer (ml O_2/min divided by ml blood flow/min × 100%). As described elsewhere,[17] a 5 vol% transfer rate is equivalent to raising blood oxygen saturation from 65% to 95%, and a 3.3 vol% transfer rate is equivalent to raising blood oxygen saturation from 75% to 95%. There are three sets of data plotted in **Figure 7**, one at each of three

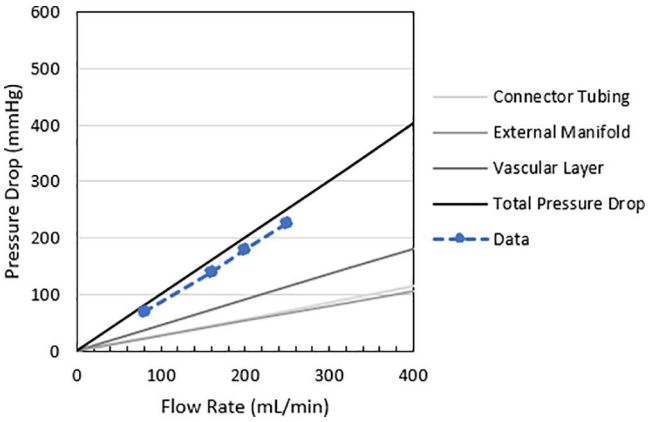

Figure 6. Measured blood pressure drop in mmHg (labeled data with blue markers) *versus* blood flow rate (ml/min) for the full eight-layer device with tubing and the external manifold. Lines represent computational model predictions for connector tubing, external tubing, eight-layer stack of devices, and the total pressure drop (dark line).

different gas flow conditions. In each case, the gas is 99.99% pure oxygen, and the oxygen flow rate is held constant as described in the Methods section. However, the diamonds (400 mmHg) and squares (200 mmHg) markers in the figure pertain to increases in the oxygen pressure in the device during testing, relative to the circles (0 mmHg oxygen pressure.) The highest oxygen pressure is represented with the orange markers, resulting in more efficient oxygen transfer across all flow rates. Even at the highest oxygen pressure, visual observation for the presence of oxygen bubbles in the blood was marginal and did not disturb the testing. To avoid the formation of gas emboli in the blood, the blood pressure should exceed the oxygen side pressure, and this is the case for almost all of the conditions tested, except for the lowest flow rates at the 200 and 400 mmHg oxygen pressure points. The raw data for this test is provided in Table S2, Supplemental Digital Content 2, http://links.lww.com/ASAIO/A770.

In **Figure 8**, we demonstrate the reproducibility of the oxygen transfer testing with a repeat test done at the lowest oxygen pressure (corresponding to the data marked by circles in **Figure 7**), with error bars reflecting the standard deviation across three repeat measurements at each flow rate.

Discussion

Microfluidic oxygenator technology possesses potential technical advantages over conventional HFM devices due to its ability to entrain blood in precisely defined, physiologically based microchannel networks throughout the circuit. Shortcomings in HFM cartridges have been partly addressed by modification and optimization of the housing region and the placement of the fiber assembly, but the fundamental inability of HFM devices to maintain smooth branching flow in a closed channel network remains. Therefore strenuous efforts have been made over the past several years to advance microfluidic systems, largely based on their ability to realize designs with very shallow blood channels and thin gas transfer membranes. While these advantages are potentially important, the techniques used to produce these devices face limitations in both the ability to generate smooth blood flow patterns at channel junctions and within distribution manifolds. Further, many aspects of the microfluidic technology are difficult to scale, given the reliance on semiconductor cleanroom processes such as photolithography and etching. Finally, standard microfluidic fabrication processes invoke patterning methods that limit channel depth to a single level, while a critical aspect of the physiologic microcirculation is the relatively symmetric increase in vessel cross-section in regions of a larger flow.

Given these challenges facing microfluidics-based technologies, we have pursued a design approach based on precision CNC machining, which has advanced rapidly in terms of minimum dimension and geometric tolerances over recent years. This technique overcomes two of the three fundamental limitations described above, namely the inability to create smooth blood flow paths at channel junctions and the restriction of microchannels to a single depth throughout an entire network. The other limitation, related to difficulties in scaling the technology toward larger blood flows, is addressed by a combination of expanded lateral blood flow network patterns and the development of techniques capable of stacking and integrating multilayer structures in a biomimetic manner. Manifold designs

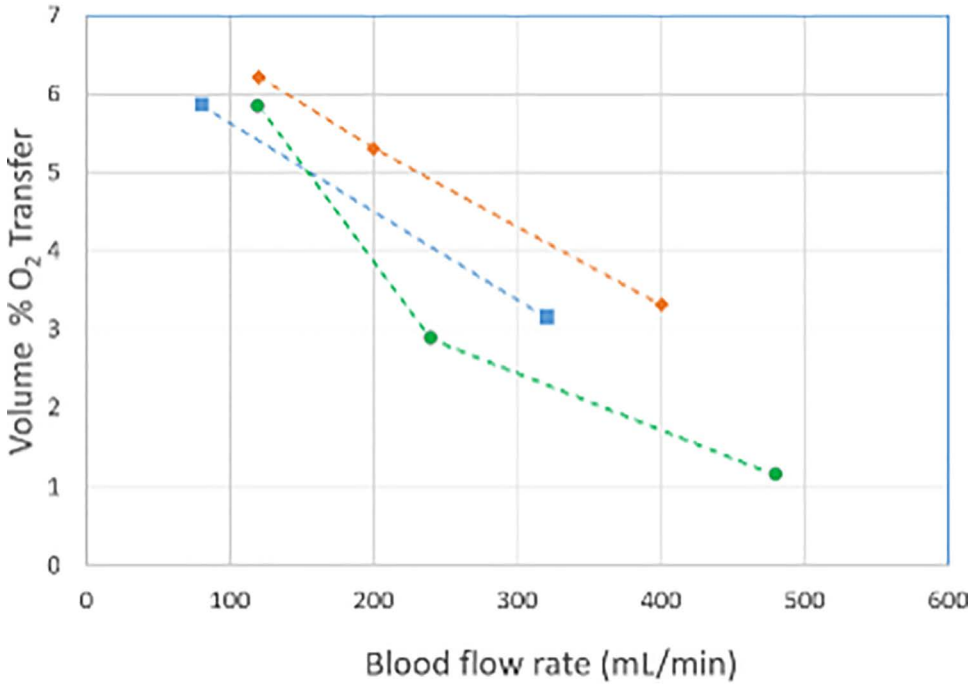

Figure 7. Blood oxygen transfer testing for eight-layer microfluidic oxygenator with volume percent oxygen transfer (O_2 transfer in ml/min divided by blood flow rate in ml/min × 100%) plotted against blood flow rate. Data represent three different oxygen flow and pressure conditions (diamonds higher than squares higher than circles); each data point represents an average of three readings taken at each blood flow rate.

and fabrication processes capable of vertically integrating multiple layers are critical aspects of this new approach.

Here, we report the first demonstration of substantially higher flow microfluidic oxygenator devices, reaching flow rates as high as 480 ml/min in a multilayer structure. We believe that these flow rates are the highest ever achieved in a complex microfluidic device. Oxygen transfer is tested in these devices across a range of gas flow conditions, with the transfer as high as 5 vol% at 240 ml/min and 3.3 vol% at 400 ml/min. This advance brings microfluidic oxygenator technology to the threshold, from a blood flow rate perspective, of the scale necessary for pediatric testing, a significant opportunity realized by the convergence of new design and fabrication techniques.

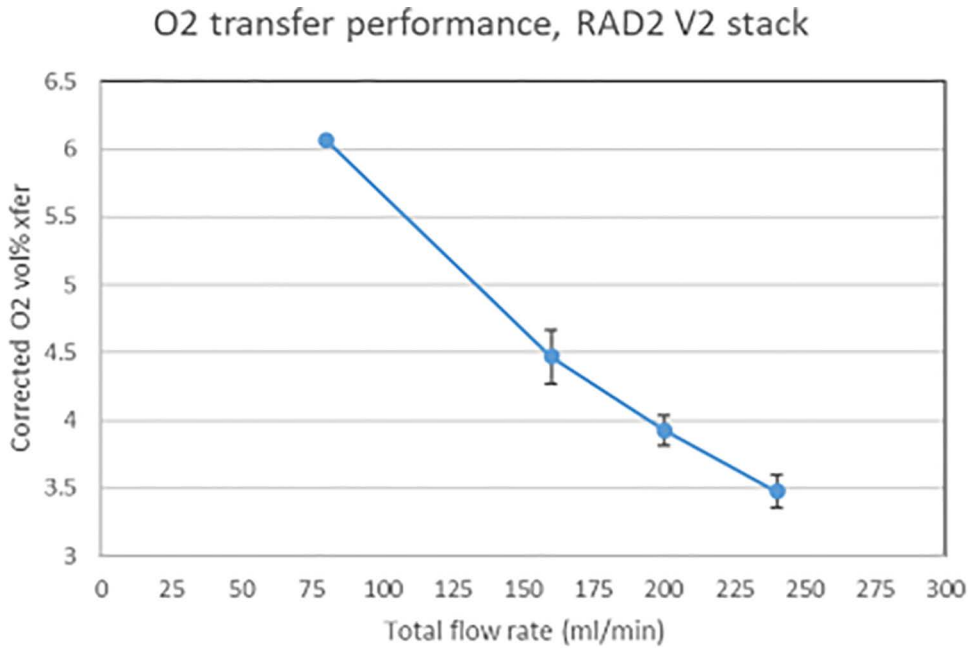

Figure 8. Blood oxygen transfer testing for eight-layer microfluidic oxygenator with volume percent oxygen transfer (O_2 transfer in ml/min divided by blood flow rate in ml/min × 100%) plotted against blood flow rate. Repeat test at lowest oxygen pressure condition (green data from **Figure 7**) with error bars indicating standard deviation of three readings at each flow rate.

The high flow rates achieved in this study are very promising, but many significant challenges remain. The blood pressure drops in these devices at high flow rates are well in excess of targeted values for clinical oxygenators (HFM oxygenator pressure drops are typically under 100 mmHg at operating flow rates), and therefore new device designs that distribute the blood flow at lower pressures while maintaining high-efficiency transfer will be needed. This technology has been shown to be capable of extremely high gas transfer efficiencies, in excess of 300 ml/min/m^2 of active membrane area, several-fold higher than for HFM devices.[17] These high pressures result in membrane distortion in the range of 10–30 microns at operational flow rates, an effect that would be addressed by reducing pressure drop in the network.

Key future requirements include the development of higher volume device manufacturing processes, potentially replacing current casting methods with injection molding or other techniques. Current construction techniques are very labor-intensive, limiting fabrication rates such that only one eight-layer device was built for this study. Also critical will be the demonstration of stable, high gas transfer rates in extended large animal studies, as well as rigorous hemocompatibility testing as a function of anticoagulant administration, requiring the ability to access large volumes of blood for extended device evaluations. More extensive studies are currently underway, along with evaluation of the integration of antithrombotic coating technologies in these microfluidic devices as a further means to mitigate potential clotting and to reduce reliance on systemic anticoagulant administration. Further developments aim to continue to ultimately scale this technology toward levels required for adult human use.

Acknowledgment

The authors gratefully acknowledge the support of the U.S. Army Medical Research Acquisition Activity, 820 Chandler Street, Fort Detrick MD 21702-5014 as an awarding and administering acquisition office. This work was supported by the U.S. Army, through the Peer-Reviewed Medical Research Program under Award No W81XWH1910518. Opinions, interpretations, conclusions, and recommendations are those of the authors and are not necessarily endorsed by the U.S. Army. The authors would also like to acknowledge the contributions of John Lachapelle and Tim Petrie of Draper for technical and programmatic support.

References

1. Patel SB, Kress JP: Sedation and analgesia in the mechanically ventilated patient. *Am J Respir Crit Care Med* 185: 486–497, 2012.
2. Fan E, Brodie D, Slutsky AS: Mechanical Ventilation during Extracorporeal Support for Acute Respiratory Distress Syndrome. For Now, a Necessary Evil. *Am J Respir Crit Care Med* 195: 1137–1139, 2017.
3. Palanzo D, Qiu F, Baer L, Clark JB, Myers JL, Undar A: Evolution of the extracorporeal life support circuitry. *Artif Organs* 34: 869–873, 2010.
4. Schoberer M, Arens J, Lohr A, *et al*: Fifty years of work on the artificial placenta: milestones in the history of extracorporeal support of the premature newborn. *Artif Organs* 36: 512–516, 2012.
5. Gray BW, Haft JW, Hirsch JC, Annich GM, Hirschl RB, Bartlett RH: Extracorporeal life support: experience with 2,000 patients. *ASAIO J* 61: 2–7, 2015.
6. Brodie D, Bacchetta M: Extracorporeal membrane oxygenation for ARDS in adults. *N Engl J Med* 365: 1905–1914, 2011.
7. Bartlett RH: Esperanza: the first neonatal ECMO patient. *ASAIO J* 63: 832–843, 2017.
8. Cornish JD, Carter JM, Gerstmann DR, Null DM Jr: Extracorporeal membrane oxygenation as a means of stabilizing and transporting high risk neonates. *ASAIO Trans* 37: 564–568, 1991.
9. Greenough A, Agha M, Smith APR: Extracorporeal membrane oxygenation for neonates. In *Neonatology: A Practical Approach to Neonatal Diseases*. New York City, NY, Springer, 2012.
10. Neff LP, Cannon JW, Stewart IJ, *et al*: Extracorporeal organ support following trauma: the dawn of a new era in combat casualty critical care. *J Trauma Acute Care Surg* 75(2 Suppl 2): S120–8; discussion S128, 2013.
11. Cannon JW, Mason PE, Batchinsky AI: Past and present role of extracorporeal membrane oxygenation in combat casualty care: how far will we go? *J Trauma Acute Care Surg* 84(6S Suppl 1): S63–S68, 2018.
12. Noah MA, Peek GJ, Finney SJ, *et al*: Referral to an extracorporeal membrane oxygenation center and mortality among patients with severe 2009 influenza A(H1N1). *JAMA* 306: 1659–1668, 2011.
13. Tavazzi G, Pellegrini C, Maurelli M, *et al*: Myocardial localization of coronavirus in COVID-19 cardiogenic shock. *Eur J Heart Fail* 22: 911–915, 2020.
14. Lang Y, Zheng Y, Li T: The treatment of extracorporeal organ support for critical ill patients with coronavirus disease 2019: a brief perspective from the front line. *Artificial Organs* 45:189–190, 2020.
15. Federspiel W, Henchir K: Lung, artificial: basic principles and current applications. In *Encyclopedia of Biomaterials and Biomedical Engineering, 2nd ed. Boca Raton, FL, CRC Press, 2008; Volume 4*.
16. Kniazeva T, Epshteyn AA, Hsiao JC, *et al*: Performance and scaling effects in a multilayer microfluidic extracorporeal lung oxygenation device. *Lab Chip* 12: 1686–1695, 2012.
17. Gimbel AA, Hsiao JC, Kim ES, *et al*: A high gas transfer efficiency microfluidic oxygenator for extracorporeal respiratory assist applications in critical care medicine. *Artif Organs* 45: E247–E264, 2021.
18. Potkay JA: The promise of microfluidic artificial lungs. *Lab Chip* 14: 4122–4138, 2014.
19. Wagner G, Kaesler A, Steinseifer U, Schmitz-Rode T, Arens J: Comment on 'the promise of microfluidic artificial lungs' by J. A. Potkay, *Lab Chip*, 2014, 14, 4122-4138. *Lab Chip* 2016. doi:10.1039/c5lc01508a.
20. Potkay JA: Reply to the 'Comment on "The promise of microfluidic artificial lungs"' by G. Wagner, A. Kaesler, U. Steinseifer, T. Schmitz-Rode and J. Arens, Lab Chip, 2016, 16. *Lab Chip* 16: 1274–1277, 2016.
21. Reyes DR, van Heeren H, Guha S, *et al*: Accelerating innovation and commercialization through standardization of microfluidic-based medical devices. *Lab Chip* 21: 9–21, 2021.
22. Kaazempur-Mofrad MR, Krebs NJ, Vacanti JP, Borenstein JT: A MEMS-based renal replacement system. Proc. 2004 Sensors and Actuators Conf., Hilton Head Is., June 2004. Cleveland OH, Transducers Research Foundation, 2004.
23. Burgess KA, Hu HH, Wagner WR, Federspiel WJ: Towards microfabricated biohybrid artificial lung modules for chronic respiratory support. *Biomed Microdevices* 11: 117–127, 2009.
24. Kung MC, Lee JK, Kung HH, Mockros LF: Microchannel technologies for artificial lungs: (2) screen-filled wide rectangular channels. *ASAIO J* 54: 383–389, 2008.
25. Potkay JA: The promise of microfluidic artificial lungs. *Lab Chip* 14: 4122–4138, 2014.
26. Hoganson DM, Pryor HI 2nd, Bassett EK, Spool ID, Vacanti JP: Lung assist device technology with physiologic blood flow developed on a tissue engineered scaffold platform. *Lab Chip* 11: 700–707, 2011.
27. Dabaghi M, Saraei N, Fusch G, *et al*: Microfluidic blood oxygenators with integrated hollow chambers for enhanced air exchange from all four sides. *J Memb Sci* 596: 117741, 2020.
28. Mohamed MGA, Kumar H, Wang Z, Martin N, Mills B, Kim K: Rapid and inexpensive fabrication of multi-depth microfluidic device using high-resolution LCD stereolithographic 3D printing. *J Manuf Mater Proces* 3: 26, 2019.
29. Santos J, Vedula EM, Lai W, *et al*: Toward development of a higher flow rate hemocompatible biomimetic microfluidic blood oxygenator. *Micromachines (Basel)* 12: 888, 2021.
30. Matharoo H, Dabaghi M, Rochow N, *et al*: Steel reinforced composite silicone membranes and its integration to microfluidic oxygenators for high performance gas exchange. *Biomicrofluidics* 12: 014107, 2018.